sent to MNRAS

Connection between the observed properties of blazar S5 0716+71 in the helical jet model

Marina S. Butuzova,[1⋆]
[1] *Crimean Astrophysical Observatory, Nauchny, Crimea, 298409, Russia*

arXiv:1609.07538v1 [astro-ph.GA] 23 Sep 2016

ABSTRACT

Based on periodic variations in the position angle of inner jet features PA_{in} of the blazar S5 0716+71 (Bach et al. 2005; Lister et al. 2013)it is assumed that the jet has a helical structure. Within this, a number of the observed properties are explained: 1) different values of long-term variability periods of radio (5.8 yrs) and optical (3.3 yrs) emission (Raiteri et al. 2003) and variations in PA_{in} values (10.9 yrs) (Lister et al. 2013); 2) alternation of time intervals with both positive and negative correlation between γ-ray flux density and PA_{in} (Rani et al. 2014); 3) difference between the apparent speeds of inner and outer jet components observed by Rastorgueva et al. (2011) and Rani et al. (2015); 4) high apparent speed of individual jet features that is $\approx 37c$ (Rani et al. 2015). We defined helical geometrical parameters, velocity and pitch angle of the jet features, physical distances from the supermassive black hole to regions where a surrounding medium becomes optically thin for radio and optical emission. The supplementary to (Bach et al. 2005; Britzen et al. 2009) evidences for non-ballistic motion of the jet matter have been obtained from the long-term variability of S5 0716+71. The influence of the jet motion nature on the observed variability periods of the flux density and PA_{in} was described theoretically. This should be taken into account in estimating the black hole mass and parameters of periodic processes in the active nuclear. We show that correlation between the observed values which correspond to different jet parts is strongly depend on the mutual orientation of these parts relative to a plane containing the helix axis and the line of sight. Results of this work do not depend on mechanisms causing the helical jet structure. The obtained theoretical formulae determining helical jet parameters can be applied to other blazars.

Key words: BL Lacertae objects: general – BL Lacertae objects: individual S5 0716+71 – jets

1 INTRODUCTION

Practically all observed blazar radiation is produced in their relativistic jet. Therefore, it is naturally to expect that not only physical processes occurred in the jet (for instance, passage of a shock wave Marscher & Gear 1985) are responsible for the flux density variability but also geometric effects. The latter ones lie in the fact that the received radiation flux density has a power-law dependence on the Doppler factor which value is sensitive to a jet feature speed and an angle between direction of the feature motion and the line of sight (see, e.g., Camenzind & Krockenberger 1992; Abraham 2000). Therefore, taking into account data obtained from the multi-wavelength photometric and radio interferometric observations we can conclude about the jet structure and motion nature of its components. This was implemented in the paper on the assumption that long-term variability is caused by variations of the Doppler factor.

The BL Lac object S5 0716+71 [$z = 0.31$ (Nilsson 2008), $0.2315 < z < 0.3407$ (Danforth et al. 2013), $z = 0.26$ (Wagner et al. 1996), $z \geq 0.52$ (Sbarufatti, Treves & Falomo 2005)] has been intensively observed in the radio, optical, X-ray and γ-ray ranges (e.g. Liao et al. 2014). It is a very variable source on both short (Montagni et al. 2006; Stalin et al. 2006; Wu et al. 1996; Vol'Vach et al. 2009; Poon et al. 2009) and long-term (Raiteri et al. 2003; Nesci et al. 2005; Dai et al. 2013) time scales. For more than ten years this object has been observed by VLBI (Bach et al. 2005; Britzen et al. 2009; Rani et al. 2015) and within the MOJAVE program (e.g. Lister et al. 2013). From these data, the inner jet position angle PA_{in} was found to vary with a period of about 10 years (Bach et al. 2005; Lister et al. 2013). This is the most easily explained by the fact that the jet has a helical structure. The geometrical parameters of the helicoid are defined

⋆ E-mail: mbutuzova@craocrimea.ru

© 2016 M.S. Butuzova

in Section 2 irrespective of processes causing a helical jet and the motion nature of jet features. The analysis of long-term observations in the radio and optical ranges gives long-term variability periods of 3.3 and 5.6-6 years (Raiteri et al. 2003; Liu et al. 2012), respectively. These values differ between themselves and they are distinct from the variability period of PA_{in}. The connection between these periods is presented in Section 3. And it is possible only for non-ballistic motion of jet components. In terms of the assumption about the helical jet, the following observed properties are explained. 1. The alternation of intervals of strong positive and negative correlation between γ-ray flux density of the blazar S5 0716+71 and PA_{in} (Section 4) detected by Rani et al. (2014). 2. The contradictory results of kinematic analysis carried out in papers (Rastorgueva et al. 2011; Rani et al. 2015) and the high apparent speed of jet components (Rani et al. 2015) (Section 5). Discussion of the obtained results and conclusions are given in Sections 6 and 7, respectively.

2 DETERMINATION OF THE JET GEOMETRICAL PARAMETERS

The blazar S5 0716+71 is remarkable because of the fact that the inner jet position angle PA_{in} shows periodic changes in its value (Bach et al. 2005; Lister et al. 2013). Thus, variation in PA of the jet part within 1 mas from the core with a period of (7.4 ± 1.5) years and amplitude of 3.5° was detected based on observations at frequencies of 5, 8.4, 15, 22 GHz during 1992.7-2001.2 (Bach et al. 2005). Lister et al. (2013) defined the period of 10.9 years and amplitude of 11° for the PA_{in} variation based on observational data obtained at frequencies of 43 and 86 GHz during 1994.5-2011.5. The precessing jet nozzle is a probable explanation of the PA_{in} periodic variation (Bach et al. 2005). However, as pointed by Lister et al. (2013), this may be caused by jet stream instabilities. In both cases the jet gets a helical structure. A number of researches are devoted to helical jets. The precessing ballistic jet was considered for OJ 287 (Abraham 2000), BL Lac (Stirling et al. 2003; Caproni, Abraham & Monteiro 2013), 3C 120 (Caproni & Abraham 2004), 3C 279 (Abraham & Carrara 1998). But this model is good for a heavy jet that contains not only electrons but also other heavy particles. The development of magnetohydrodynamic instabilities is possible in a light leptonic jet (Ferrari, Trussoni & Zaninetti 1981; Hardee &Norman 1988; Birkinshaw 1991; Hardee 2000; McKinney & Blandford 2009). In magnetic jets the helical structure is formed by twisting magnetic field filaments inside and outside the conical jet (Meier 2001). Also plasma has a helical trajectory of motion near the magnetized accretion disk (Camenzind & Krockenberger 1992). Note that the obtained results do not depend on processes causing the helical jet structure.

The jet is represented by individual components moving with the same speed. These components can be both plasmoids and shock wave fronts. We assume that the jet matter lies on the surface of an imaginary cone and forms a helix originating at some distance d_0 from the cone apex (Fig. 1).

A coordinate system with the beginning at the cone apex is introduced. Note that point O may not coincide with position of the supermassive black hole or position of the jet physical beginning. The coordinate axes are placed in such a way as to the axis OZ is directed along the line of sight and the axis OX – along the projection of the cone axis OA onto the plane of the sky. The half-opening angle of the cone and angle between cone axis and the line of sight are denoted by ξ and θ_0, respectively. At each epoch Lister et al. (2013) detected PA_{in} as a flux density-weighted position angle average of all components in the annular region from 0.15 to 1 mas from the core. Unlike them, for simplicity, we take that the position angle of inner features is measured at the moment of their reaching the distance d from the cone apex. The second value setting the feature position on the cone's surface is the azimuth angle φ which is defined as an angle between planes OXZ and OAB. When the jet moves outside, the angle φ of each subsequent feature reaching the distance d differs from the previous one. This causes variations in PA_{in}. When $\theta_0 < \xi$ the line of sight lies inside the jet helicoid. Then, over the period of φ variations the value of the inner jet position angle PA_{in} varies by 360°. This is not in agreement with observational data on the blazar S5 0716+71 (Bach et al. 2005; Lister et al. 2013). Therefore, in this paper we consider only the case of $\theta_0 > \xi$.

The mean value of the inner jet position angle PA_0 corresponds to location of the feature in the plane OXZ. ΔPA is the angle between the axis OX and radius-vector of the feature projected onto the plane of the sky. As is seen in Fig. 1, the expression for ΔPA through φ, θ_0, ξ can be easily obtained from projections OA, AC, BC onto the plane of the sky:

$$\Delta PA = \frac{\sin\xi\,\sin\varphi}{\cos\xi\,\sin\theta_0 + \sin\xi\,\cos\theta_0\,\cos\varphi} \approx \frac{\sin\varphi}{\theta_0/\xi + \cos\varphi}. \quad (1)$$

And the observed position angle is $PA_{in} = \Delta PA + PA_0$. Expression (1) is similar to the formula for difference in position angles of parsec-scale and kiloparsec-scale jets in a simple bend model (Conway & Murphy 1993). In the latter case θ_0 is the angle between initial direction of the parsec-scale jet and ξ is the bend angle of the jet. If θ_0 and ξ values are small then PA_{in} depends on the ratio θ_0/ξ. Fig. 2 shows PA_{in} variation calculated by the accurate Formula 1 over one period for different values of the ratio θ_0/ξ. It is seen that if the θ_0/ξ increases then both the amplitude of PA_{in} variability and curve skewness decrease. Note, that in the observed reference frame variations of φ are not uniform with time.

By Expression 1 it follows that minimum and maximum PA_{in} values occur at

$$\varphi = \pm \arccos\left(-\tan\xi\,\cot\,\theta_0\right). \quad (2)$$

Inserting (2) into (1) and substituting $\sin\varphi = \sqrt{1-\cos^2\varphi}$ we found the amplitude of PA_{in} variations:

$$PA_{max} = \arctan\left(\sin\xi\left(\cos^2\xi\,\sin^2\theta_0 - \sin^2\xi\,\cos^2\theta_0\right)^{-1/2}\right) \approx$$
$$\approx \left((\theta_0/\xi)^2 - 1\right)^{-1/2}. \quad (3)$$

It is clear that if θ_0 and ξ angles are small the amplitude depends on their ratio too. Lister et al. (2013) have obtained a sufficient series of observations with better angular resolution than Bach et al. (2005), therefore results of Lister et al. (2013) are used in this paper. Since $PA_{max} = 11^\circ$ then from (3) it follows that $\theta_0/\xi \approx 5.3$. Several determinations

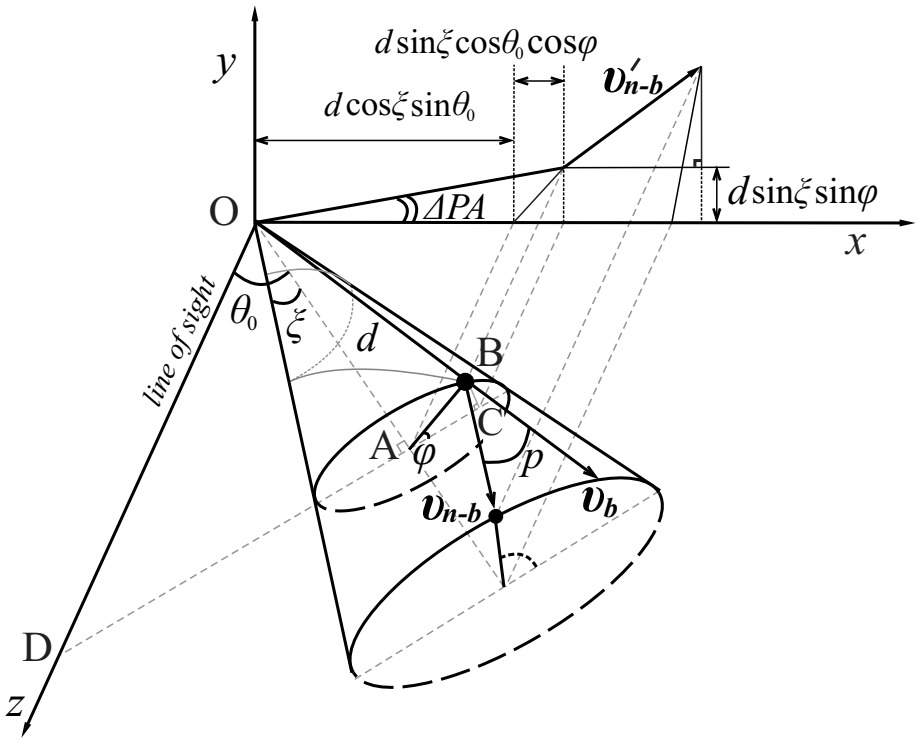

Figure 1. Scheme for geometrical parameters of the helical jet. Letter "B" marks position of the feature at the distance d from the cone apex at the certain point of time. The projection onto the plane of the sky is marked by prime. The velocity vectors are shown for both ballistic (along the cone generator) $\boldsymbol{\upsilon_b}$ and non-ballistic $\boldsymbol{\upsilon_{n-b}}$ motion of the jet feature. In the latter case the velocity vector $\boldsymbol{\upsilon_{n-b}}$ is directed at the angle p to the cone generator.

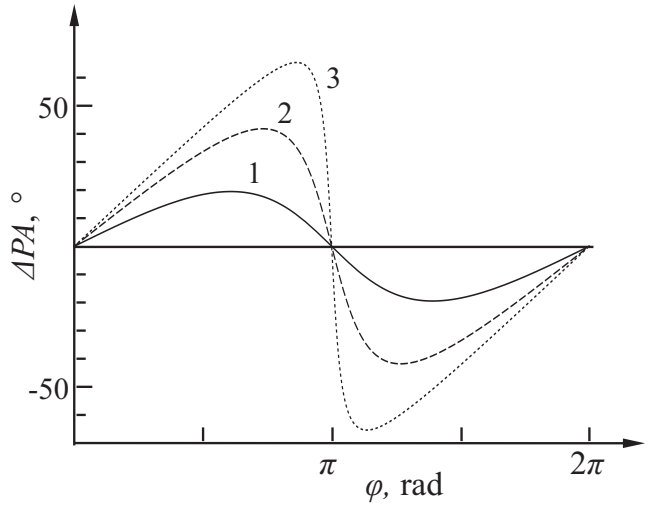

Figure 2. Theoretical deviation of the inner jet position angle from the mean value over the period for different values of the ratio θ_0/ξ: 1) 3; 2) 1.5; 3) 1.1.

of the S5 0716+71 jet angle with the line of sight give an interval of values for θ_0 from 0.5° to 11° based on the apparent speed of VLBI/A-jet components (Rastorgueva et al. 2009, 2011; Nesci et al. 2005; Britzen et al. 2009). But these estimations were made based on observations over a small time interval and they depend on authors' notion about the jet. Therefore, we use a value obtained by Pushkarev et al. (2009). Note that almost the same value θ_0 was obtained by Savolainen et al. (2010). Pushkarev et al. (2009) estimated $\theta_0 = 5.3°$ from the maximum apparent speed of the jet component that has a radial motion without acceleration and having been observed within the MOJAVE program for no less than 5 epochs. According to (3) $\xi \approx 1°$. When determining jet opening angles by VLBA-maps of the sources Pushkarev et al. (2009) obtained a value of $2\xi \approx 1.59°$ for S5 0716+71. Thus, there is a good agreement between values of half-opening angles of the blazar S5 0716+71 jet defined by different independent ways.

3 CONNECTION BETWEEN LONG-TERM VARIABILITY PERIODS OF DIFFERENT OBSERVABLE VALUES

The many-year light curves of the blazar S5 0716+71 in the radio and optical ranges indicate the existence of long-term variability periods. Raiteri et al. (2003) found long-term variability periods in the optical and radio wavebands by applying the Discrete Fourier Transform. The period of 3.3 years is in the optical (Raiteri et al. 2003; Gupta et al. 2008), while 5.6-6 years – in the radio band at frequencies of 14.5 and 15 GHz (Raiteri et al. 2003), 5.8±0.4 at 15 GHz (Liu et al. 2012). The analysis of data for more than 30-year observation spell at frequencies between 4.8 and 36.8 GHz also shows the existence of both the almost 8-year period and periods of shorter duration (Bychkova et al. 2015). There-

fore, on the one hand, the absence of equal variability periods of radio and optical emission indicates that physical processes occurred in the jet are responsible for brightness variations. On the other hand, periodic changes of the inner jet position angle point to periodic variations of the jet direction what must be reflected in multi-waveband variability of S5 0716+71. But this is absent. Let us find out the cause of this contradiction within the assumption about the jet helical structure. To retain the helical structure for a rather long time we assume through this paper that jet components move with the same and constant speed.

Based on observational results (see, e.g., Fuhrmann et al. 2014), regions emitting the received γ-ray and optical emission are at less distance from the black hole than the VLBI/A-core. This is because the observed γ-ray emission comes from the region which medium is not transparent for radiation at lesser frequencies. With moving away from the active nucleus, parameters of the medium change and the medium becomes optically thin for large wavelength emission (Blandford & Konigl 1979). Therefore, we assume that the medium becomes transparent for optical emission of the jet feature when this feature reaches circle '1' (Fig. 3).

This circle is formed by intersecting the cone's surface with plane '1' which is orthogonal to the cone's axis and placed at the distance $d_1 \cos\xi$ from the cone apex. While further outward moving, the jet component reaches the analogous circle '2' placed at the distance $d_2 \cos\xi$. In this region the medium becomes transparent for radio emission. Moving further, the component reaches circle '3' placed at the distance $d_3 \cos\xi$ and appears on VLBA-maps as the innermost feature to the core. The PA_{in} is measured at this distance. We assume that the long-term variability is caused by changes of the Doppler factor

$$\delta = \sqrt{1-\beta^2}\,(1-\beta\cos\theta)^{-1}\,, \tag{4}$$

where β is the physical speed of a jet feature in units of the speed of light, θ is the angle between the line of sight and velocity vector of the feature. Let us introduce a fictitious point moving along circle '1' ('2' or '3') in such a way that its position coincides with position of the jet component intersecting this circle at the certain point of time. Then periods of radio, optical and PA_{in} variability are equal to rotation periods of these fictitious points along circles '1', '2' and '3', respectively.

3.1 Ballistic jet

First we consider a case of ballistic motion of jet components. Let us represent the jet as n successive components. The difference of azimuth angles of each two adjacent features is φ, therefore, $n\varphi = 2\pi$. Changes of the Doppler factor caused by variations in θ are neglected because their sum over the period is zero. Time in the observed reference frame between moments of passing by any two adjacent features through circle '1' is denoted by Δt_1. Over this time the fictitious point moving along circle '1' describes an arc of φ degrees. Thus, the period of optical variability is equal to

$$P_1 = \Delta t_1 n. \tag{5}$$

Then the considered features intersect circle '2'. Due to the nature of motion (Fig. 4), their azimuth angles do not change. The number of features intersecting circles '1' and '2' over the period is constant too. If there is no deceleration of features between planes '1' and '2' then time intervals are $\Delta t_1 = \Delta t_2$. Hence, the period of radio variability must coincide with the period of optical one. Since it is not observed then we assume that the speed of features intersecting plane '2' is equal to $\beta_2 = a\beta_1$, herewith $0 < a < 1$ and $a > |\beta_2|$ (otherwise $\beta_1 > 1$). Time intervals in the source's reference frame between moments of intersecting circle '1' and circle '2' by any two adjacent components are equal

$$\Delta t'_1 = \Delta t'_2. \tag{6}$$

The interval between two events in the observer's reference frame is δ times less than the interval in the source's reference frame

$$\Delta t' = \delta \Delta t. \tag{7}$$

Since the Doppler factor depends on the speed of the jet feature β (4) and $\beta_1 \neq \beta_2$, in the observer's reference frame $\Delta t_1 \neq \Delta t_2$. According to (5-7)

$$\frac{P_1}{P_2} = \frac{\Delta t_1}{\Delta t_2} = \frac{\Delta t'_1\,\delta_2}{\Delta t'_2\,\delta_1} = \frac{\delta_2}{\delta_1}. \tag{8}$$

Taking into account $P_1 = 3.3$ years, $P_2 = 5.8$ years and Formula (4), we solve Equation (8) relative to a for values $\beta_1 = 0.3 - 0.9999$ (they correspond to the Lorenz factor $\Gamma = 1 - 70$). One root of the equation is always greater than unity. When $\beta_1 < 0.52$ the second root has negative values and when $\beta_1 \geq 0.52$ it satisfies our conditions. The highest value is $\beta_2 \approx 0.957$ when $a \approx 0.961$ and $\beta_1 = 0.9957$, what corresponds to $\Gamma = 3.45$. Based on observations of superluminal motion of the S5 0716+71 jet components, the Lorenz factor is $\Gamma = 10 - 20$ (see, for example, Bach et al. 2005; Montagni et al. 2006; Nesci et al. 2005; Pushkarev et al. 2009). Thus, the ballistic jet cannot give the observed difference in radio, optical and PA_{in} variability periods.

3.2 Non-ballistic jet

Consider a helical jet which features have non-ballistic motion. Let p denote the pitch angle (angle between the cone generator and velocity vector of the jet feature), ψ is the angle between the tangent to the jet helix and the cone generator at the certain point (Fig. 5). If $p = \psi$ then the jet seems to be spatially stationary and it intersects planes '1', '2' and '3' constantly at the same points, correspondingly. In such a case all the mentioned periods must be absent. If $p \neq \psi$ then we can observe the helix rotating around its axis. The rotation period depends on β and p, but does not depend on ψ.

Let us find the azimuth angle change $\Delta\varphi$ for a small time interval Δt. As is seen from Fig. 6 $\tan\varphi \approx \Delta\varphi \approx$ CD/AC, where CD$= \upsilon\Delta t \sin p$, AC$= d\,(t)\sin\xi$. Hence,

$$\Delta\varphi = \frac{\upsilon\Delta t \sin p}{d\,(t)\sin\xi}, \tag{9}$$

where $\upsilon = \beta c$ is the physical speed of the feature, $d\,(t) = d_0 + \upsilon t\cos p$ is the distance from the cone apex to the feature at the point of time t, d_0 is the distance from the cone apex at which both helical structure and non-ballistic motion of features begin. From (9) it is seen that $\Delta\varphi$ decreases with

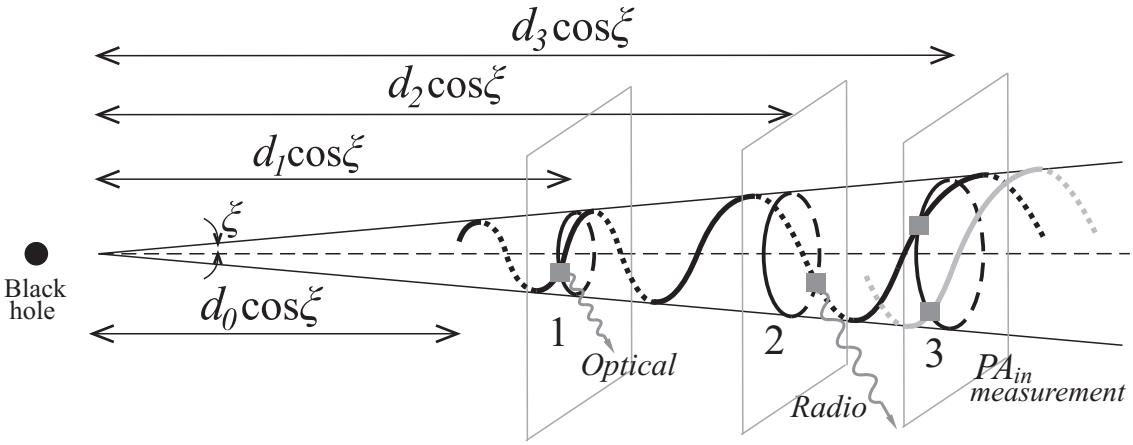

Figure 3. Locations of regions responsible for the observed optical (circle '1') and radio (circle '2') fluxes and PA_{in} (circle '3'). The bold black line shows the helical jet at the certain point of time. The helicoid begins at some distance d_0 from the cone apex. The solid line marks jet parts on the surface of the imaginary cone faced to the observer and the dashed line shows jet parts on the reverse side of the cone. The grey curve shows position of the jet part located nearby circle '3' at some subsequent point of time. It is obvious that the intersection point of the jet and circle '3' (grey square) has shifted (similarly for circles '1' and '2'). Over the variability period of the corresponding value this point moves along the whole circle and returns to the initial position.

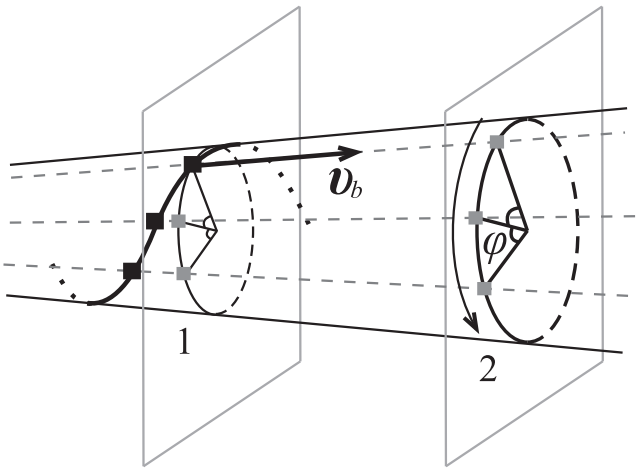

Figure 4. Scheme for the interpretation of variability periods. Several jet components are shown by black squares. For ballistic motion the trajectory of each component lies along the cone generator (dashed lines). Grey squares mark locations where these components intersect circle '1' ('2'). Arrow shows direction of moving fictitious points along circles '1' and '2'.

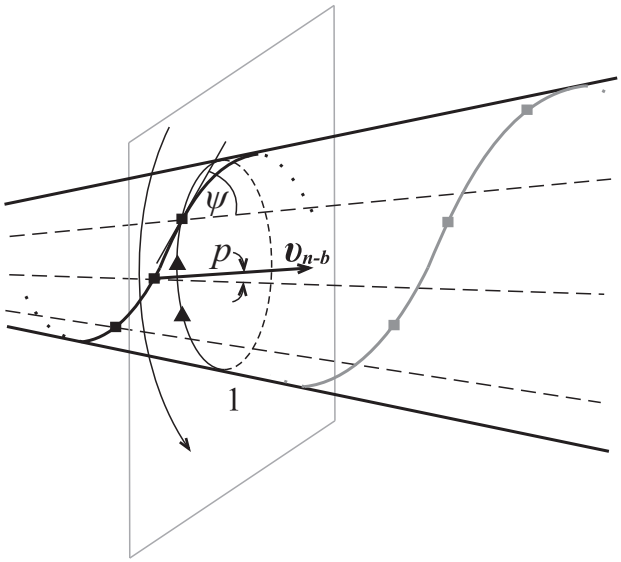

Figure 5. Scheme of the non-ballistic helical jet. Each jet feature (denoted by the filled square) moves at the angle p to the cone generator (dashed line). The angle ψ is measured between the cone generator and tangent to the helix at the given point. When $\psi = p$ features always move along the helix marked by black color. At this case the jet is spatially stationary. Grey color shows position of the helix and features at some subsequent point of time when $\psi \neq p$. The helical jet is seen as though to rotate around its axis. Filled triangles on circle '1' mark places where the jet features intersect plane '1'. The arrow shows direction of moving the fictitious point along circle '1'.

increasing d. However, we are interested in the rate of the azimuth angle change at the constant distance d_i from the cone apex to circle 'i' which corresponds to location of the region giving the main contribution to optical (i=1), radio (i=2) emission or the region where the jet feature becomes accessible for PA_{in} measurement (i=3) (see Fig. 3).

Then the angular frequency of the fictitious point moving along circle 'i' is expressed as

$$\omega_i = \frac{\Delta\varphi}{\Delta t} = \frac{\upsilon \sin p}{d_i \sin\xi}, \tag{10}$$

where $d_i = d(t_i)$, t_i - the time elapsed from the start of feature's motion and needed to reach circle 'i'. Since the rotation period of the fictitious point along circle 'i' is equal to $P_i = 2\pi/\omega_i$, then from (10) it follows that the ratio of periods of two observed values i and k is equal to the ratio of distances from the cone's apex to the jet region where the corresponding value becomes accessible for observations:

$$\frac{P_i}{P_k} = \frac{d_i}{d_k}. \tag{11}$$

Inserting various pairs of the known variability periods for S5 0716+71 into Formula (11) we obtain three independent

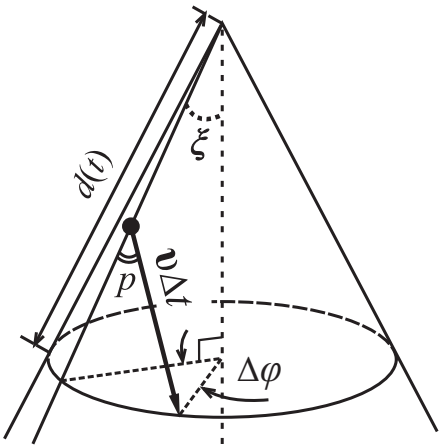

Figure 6. Change of the azimuth angle of the jet feature with time.

expressions:

$$\begin{aligned} d_2 &= 1.76\ d_1 \\ d_3 &= 3.30\ d_1 \\ d_3 &= 1.88\ d_2. \end{aligned} \qquad (12)$$

From two last equations in (12) we find that $d_2/d_1 \approx 1.76$. The ratio d_2/d_1 taken from the first expression in (12) is of the same value. Thus, there is a good agreement between the observed periods of long-term radio, optical and PA_{in} variabilities. This confirms non-ballistic jet motion when $p \neq \psi$ and the absence of jet features' deceleration at the considered distances from the core. Let us assume that PA_{in} is measured at the same distance from the VLBA-core equal to 0.5 mas. Then $d_3 - d_2 = 0.5$ mas. Using the third equation in (12) we find the distance from the cone apex to position of the VLBA-core equal to 2.51 pc. It should be taken into account that 1 mas corresponds to 4.421 pc in the ΛCDM-model with $H_0 = 71$ km/s/Mpc, $\Omega_m = 0.27$, $\Omega_\Lambda = 0.73$ (Komatsu et al. 2009) and the redshift of S5 0716+71 is z=0.3. The obtained value agrees with the distance of the VLBA-core from the black hole that is equal to 6.68 pc. This was defined by Pushkarev et al. (2012) at the frequency of 15.4 GHz. This correspondence gives additional evidence in favour of our assumption about the jet.

4 CORRELATION BETWEEN THE EMISSION FLUX AND THE INNER JET POSITION ANGLE

The ballistic jet motion was ruled out because of there is distinction between variability periods of different observed values. Let us ascertain whether it is possible from the analysis of correlation of the flux density and PA_{in} to conclude about the nature of the jet features' motion.

4.1 Ballistic motion

The expression for the angle θ between the line of sight and velocity vector of the jet feature can be obtained from triangles OBD and ABD (Fig. 1):

$$\cos\theta = \cos\xi\ \cos\theta_0 - \sin\xi\ \sin\theta_0\ \cos\varphi. \qquad (13)$$

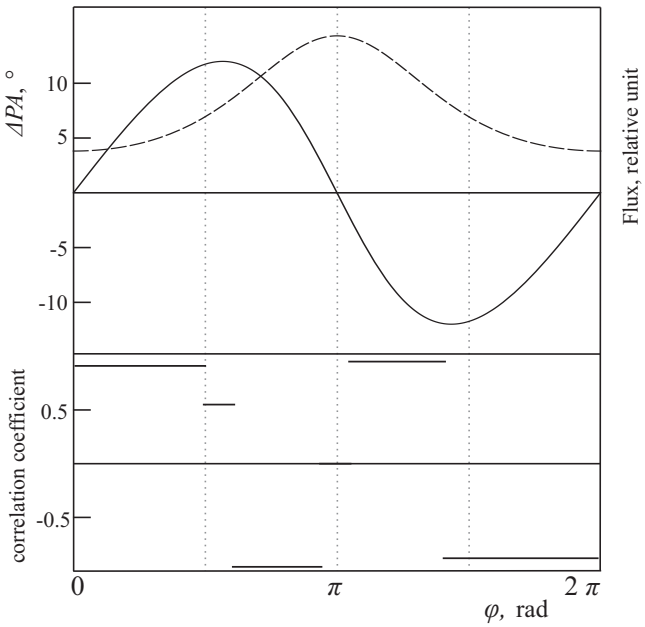

Figure 7. Deviations of the inner jet position angle from the average value ΔPA (solid line) and observed flux density F_ν (dashed line) over the period (top panel) and correlation coefficient κ between these values (bottom panel) for a case of ballistic motion of helical jet features.

Within the assumption that only geometrical effects produce long-term variability, the flux density depends on the Doppler factor as:

$$F_\nu \propto \nu^{-\alpha} \delta^{3+\alpha}, \qquad (14)$$

where α is the spectral index of emission, ν is the observed frequency.

The top panel of Fig. 7 shows calculated by formulae (1), (13), (14) variations of the inner jet position angle ΔPA (when $\theta_0/\xi = 5.3$) and F_ν (when α=0.5 and $\beta = 0.995$, what corresponds to $\Gamma = 10$) depending on the value of φ. The flux density is normalized so that to make its variations accessible for visual comparison with ΔPA. The obtained curves were divided into several parts by φ in such a way that at each of them both curves do not undergo strong qualitative changes of their behaviour. From Formulae (1), (13) and (14) the arrays of ΔPA and F_ν values at varying φ with a step of 0.5° were constructed for these parts. Then, for each part the correlation coefficient κ of these arrays among themselves was found. The κ has the maximum possible value since in contrast to the observed data no measurement errors are present. The bottom panel in Fig. 7 shows values of κ for each interval. The alternation of intervals of strong positive and negative correlations is seen. The correlation coefficient has intermediate values for a rather short time. Qualitatively this theoretical result is in agreement with the result acquired by Rani et al. (2014). To explain it, Rani et al. (2014) assume a helical jet rotating around its axis. That is such the jet we concluded about in Section 3.2.

4.2 Non-ballistic motion

If the feature moves at the angle p to the cone generator, the expression for the angle between the line of sight and velocity vector of the jet feature $\boldsymbol{\upsilon_{n-b}}$ can be obtained from the expression (see Fig. 1):

$$\sin\theta = \left|\boldsymbol{\upsilon'_{n-b}}/\boldsymbol{\upsilon_{n-b}}\right|, \tag{15}$$

where $\boldsymbol{\upsilon'_{n-b}}$ is the projection of $\boldsymbol{\upsilon_{n-b}}$ onto the plane of sky. As is seen in Fig. 1, $\left|\boldsymbol{\upsilon'_{n-b}}\right|$ can be easily found:

$$\left|\boldsymbol{\upsilon'_{n-b}}\right| = \sqrt{f_1^2 + f_2^2}, \tag{16}$$

where

$$f_1 = (d + \Delta d)\sin\xi\sin\varphi_e - d\sin\xi\sin\varphi_b, \tag{17}$$

$$f_2 = (d + \Delta d)\left(\sin\xi\cos\theta_0\cos\varphi_e + \cos\xi\sin\theta_0\right) - \\ - d\left(\sin\xi\cos\theta_0\cos\varphi_b + cos\xi\sin\theta_0\right), \tag{18}$$

φ_b and φ_e are azimuth angles of points that correspond to beginning and end of segment $\left|\boldsymbol{\upsilon_{n-b}}\right|\Delta t$, respectively, Δd is value by which the distance of the feature from the cone apex increases with time Δt. We suppose that $\Delta\varphi = \varphi_e - \varphi_b$ is small. Then, taking into account (9), (16) and substituting $\varphi_e = \varphi_b + \Delta\varphi$, we obtain:

$$\sin\theta = \sqrt{g_1^2 + g_2^2}, \tag{19}$$

where

$$g_1 = \cos p\sin\xi\sin\varphi_b + \sin p\cos\varphi_b, \tag{20}$$

$$g_2 = \cos p\left(\cos\xi\sin\theta_0 + \sin\xi\cos\theta_0\cos\varphi_b\right) - \\ - \sin p\cos\theta_0\sin\varphi_b. \tag{21}$$

If $\varphi_e - \varphi_b < 0$ then signs in front of summands $\sin p\cos\varphi_b$, $\sin\xi\cos\theta_0\cos\varphi_b$ change into opposite ones. However, the consequent conclusions do not depend on the value $\varphi_e - \varphi_b$.

Showing graphically $\theta\,(\varphi)$ by Formula (19) for different p values it was found that θ values are within $\approx p \pm 5^\circ$. In order to see changes of the jet orientation in emission flux variations it is necessary that the θ is to be small. Hence, we may assume that $p \approx \theta \approx 5^\circ$ (see Section 2).

By analogy to the procedure described in Section 4.1 and taking into account the same parameters, we plot variations in ΔPA, F_ν and κ (black lines in Fig. 8). It was found that in this case the strong positive correlation between the inner jet position angle and observed emission flux density must be present constantly (see middle panel in Fig. 8). We should note that in our model observed values are produced at different distances from the black hole (Section 3). Therefore, we can almost confidently suppose that the azimuth angles of features, for which F_ν and PA_{in} are observed at the certain point of time, differ by some value of $\Delta\varphi$. To obtain a picture conformed with Rani et al. (2014) it is necessary that $\Delta\varphi \approx 79^\circ$ (grey lines for F_ν and bottom panel for κ in Fig. 8). On the other hand, from Fig. 7 it follows that if $\Delta\varphi \approx \pi/2$ or $\approx \pi$ then the strong positive or negative correlation is always observed, correspondingly. Hence, firstly, the difference of azimuth angle values can essentially change the correlation picture of the observed PA_{in} and F_ν values. Secondly, by correlation between F_ν and PA_{in} it is impossible to define the nature of motion of individual helical jet features.

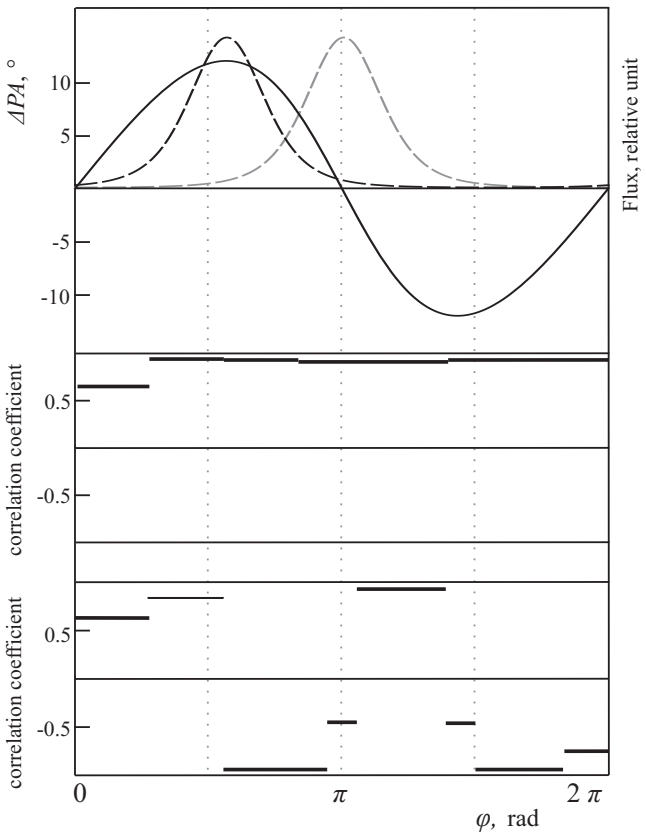

Figure 8. Variations of the inner jet position angle relative to its average value ΔPA (solid line) and observed flux density F_ν (dashed line) over the period (top panel) and correlation coefficient κ between these values for $\Delta\varphi = 0^\circ$ (middle panel) and for $\Delta\varphi = 79^\circ$ (bottom panel) in the case of non-ballistic motion of helical jet features. Black dashed curve corresponds to zero difference between azimuth angles φ of features responsible for the observed flux F_ν and the inner jet position angle PA_{in}. Grey dashed curve corresponds to the case when φ of the feature responsible for F_ν is greater by $\approx 79^\circ$ than φ of the feature for which PA_{in} is measured.

5 APPARENT MOTION OF S5 0716+71 JET COMPONENTS

The results of kinematics studying of the blazar S5 0716+71 jet are contradictory. Based on observations over 1992.73-2001.17 Bach et al. (2005) report about radially fast-moving features (the apparent speed is $\beta_{app} = 5c - 16c$). Whereas typical values for BL Lac objects are $\beta_{app} \leq 5c$ (Gabuzda, Pushkarev & Cawthorne 2000). Based on data over 1992.73-2006.32 Britzen et al. (2009) reveal no essential outward motion of components but, conversely, they discover stationary components. That is, over the whole period of observations, the jet features are at nearly the same distance from the core and have non-radial motion, i.e. their position angle varies but within measurement errors. When analysing data over 2008-2010 Rani et al. (2015) detect that the apparent speed of inner jet features (up to ~ 0.15 mas from the core) is of values up to $10c$. These are less than β_{app} values recorded in the outer jet ($> 20c$). But Rastorgueva et al. (2011) obtain a contrary result based on data over 2004. Components of the inner jet move fast,

right up to $\beta_{app} \approx 19.4c$, while the highest apparent speed of outer jet features is $10c$.

Consider the results listed above within the framework of the helical jet model. According to Rastorgueva et al. (2011) values of the inner jet PA were close to maximum ≈25°, and position angles of the outer jet were of almost minimum values ≈15°. From (2) it follows that azimuth angles of the inner and outer jet features are approximately equal to $\varphi_{fast} = 101°$ and $\varphi_{slow} = 259°$, respectively. Rani et al. (2015) used data taken over the interval 09.2008-10.2010. By this time, features being inner in 2004 had gone to the outer part of the jet and the inner jet PA has the minimum value (see Fig. 8 from Lister et al. 2013). Thus, for 2008-2010 the azimuth angle values of the inner and outer features are about φ_{slow}=259° and φ_{fast}=101°, respectively. According to results of kinematics studying of features over the interval 1992.72-2001.17 Bach et al. (2005) note that components of the inner jet systematically move slower than that of the outer jet. Taking into account that in 1997-1998 the PA_{in} had the minimum values, this result is in agreement with the following conclusion. In both 2004 and 2008-2010, the fast-moving features have the azimuth angle of 101° and slowly-moving features – 259°. At the constant physical velocity β of features, the θ-angle value affects the value of the apparent speed $\beta_{app} = \beta \sin\theta / (1 - \beta\cos\theta)$. At the mentioned azimuth angles, the ballistically moving jet components have similar values $\theta_{fast} = \theta_{slow} \approx 8°$ (13). For non-ballistic motion (19) $\theta_{fast} \approx 3°$ and $\theta_{slow} \approx 13°$ (for $p = 5°$). Therefore, only in the case of the non-ballistic jet, the discrepancy in azimuth angle values of inner and outer features at different observational epochs naturally explains prima facie contradictory results of the kinematic analysis of the blazar S5 0716+71 jet obtained by Rastorgueva et al. (2011) and Rani et al. (2015).

Fig. 9 shows the dependence of the ratio between apparent speeds of inner and outer jet components on the pitch angle for the epoch 2008-2010

$$r_{app} = \frac{\beta_{app\,out}}{\beta_{app\,in}} = \frac{\sin\left(\theta\left(\varphi_{out}\right)\right)\left(1 - \beta\cos\theta\left(\varphi_{in}\right)\right)}{\sin\left(\theta\left(\varphi_{in}\right)\right)\left(1 - \beta\cos\theta\left(\varphi_{out}\right)\right)}. \qquad (22)$$

The observed value $r_{app} \approx 2$ (Rani et al. 2015) is seen to be reachable only if the jet speed is $\beta \geq 0.999$. Wherein, the pitch angles may approximately be equal to 2, 4.5, 5.5 and 14°. Substituting these values into Expression (19) we get that only when $p = 5.5°$ the θ varies within the interval from 0.5° (Britzen et al. 2009) to 11° (Rastorgueva et al. 2011) that corresponds to existing estimation of the θ. When $\theta = 1-2°$ and $\beta = 0.999 - 0.9995$ the high values of $\beta_{app} = 20c - 30c$ are achieved. These values were detected in the blazar S5 0716+71 jet (Rani et al. 2015).

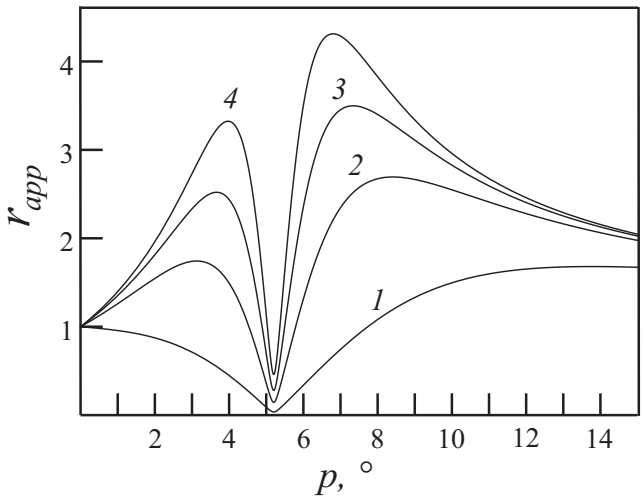

Figure 9. The apparent speed ratio of outer and inner jet components for the epoch 2008-2010 depending on the pitch angle p. The graphs are plotted for β equal to 0.995 (1), 0.999 (2), 0.9995 (3) and 0.9997 (4) (the corresponding Lorenz-factors are 10, 22, 32 and 41).

6 DISCUSSION

There are many researches showing that the jet helical structure can be produced either as a result of the black hole precession or the action of magnetohydrodynamic instabilities (Birkinshaw 1991). The apparent motion of superluminal jet components and long-term brightness variations are accounted for by the helical jet arising as a result of the black hole precession (Abraham & Carrara 1998; Abraham 2000; Stirling et al. 2003; Caproni & Abraham 2004; Caproni, Abraham & Monteiro 2013). The shape of spectral energy distribution of the blazar Mrk 501 and its variations also find explanation under the assumption about the helical jet (Villata & Raiteri 1999). The two-peaked light curve of the blazar OJ 287 is interpreted by a double helical jet that originates from precession in the binary black hole system (one of the first investigation Pietilä 1998). Therefore, it is naturally to assume that the blazar S5 0716+71 has a helical jet. This is confirmed by the observed periodic change of the inner jet position angle PA_{in} (Bach et al. 2005; Lister et al. 2013). From the analysis of the optical light curve Nesci et al. (2005) conclude about the precessing blazar S5 0716+71 jet. For a good explanation of the multi-wavelength behaviour of S5 0716+71 Opt/γ flares Rani et al. (2015) and Larionov et al. (2013) suppose that a shock wave moves along the bent, possibly, helix, trajectory. In this paper, taking into account the period and amplitude of the PA_{in} variations (Lister et al. 2013), we obtain geometrical parameters of the imaginary cone with jet matter on its surface (Section 2). This result does not depend on the fact whether jet components move ballistically or not. The found value of the cone's half-opening angle agrees well with the jet opening angle defined from VLBA-maps (Pushkarev et al. 2009). On the one hand, this confirms the validity of our assumption about the jet geometry. On the other hand, this proves that geometric effects affect substantially the variability of emission flux density from S5 0716+71. Raiteri et al. (2003) come to the same conclusion based on the analysis of long-term data on optical variability. They report that, first, the optical color index weakly correlates with brightness; second, the amplitude of variability is proportional to the magnitude what can be easily explained by variations of the Doppler factor. Also, different values of the apparent speed of jet components and difference of their position angles evidence in favour of the geometric interpretation of long-term variability of the blazar S5 0716+71 (Bach et al. 2005). It is worth noting that there is a contrary conclusion as well. Based

on B-, V-, R- optical observations Wu et al. (1996) detected that S5 0716+71 shows the blue-when-brighter chromatism what is attributable to variability caused by shock waves passing downstream along the jet flow. However, the color index behaviour requires further comprehensive study as it can be influenced by differences in step and amplitude of variability at different frequencies.

From the analysis of radio and optical variability (Raiteri et al. 2003), periods shorter than the PA_{in} variation period are detected, 3.3 and 5.8 years, respectively. Furthermore, the variation period of each of the listed three values does not reveal itself in variations of two other values. Within the helical jet model their agreement between themselves is possible only when the angle p between the features' speed vector and cone generator exists. It has been obtained that the ratio of the observed periods is equal to the ratio of the corresponding distances d from the cone's apex to the jet region where the corresponding value becomes accessible for observations. Comparing periods of radio and optical emission and PA_{in} variations we have three independent equations for d_1, d_2, d_3, and their solutions are in good agreement. Furthermore, suggesting that PA_{in} is measured at the same angular distance from the VLBA-core equal to 0.5 mas and taking into account that 1 mas corresponds to 4.421 pc we have estimated the physical distance from the VLBA-core to the cone's apex. The found value agrees with the distance from the VLBA-core to the black hole obtained on measurements of the VLBA-core shift based on observations at different radio frequencies (Pushkarev et al. 2012). That is from the variability periods we obtained evidences in favour of the helical structure of the S5 0716+71 jet and non-ballistic motion pattern of its features.The latter is also confirmed by the detected non-radial motion of VLBI-jet components (Bach et al. 2005; Britzen et al. 2009).

In Section 3 we come to a conclusion that the angle p is not equal to the angle between the tangent to the jet matter and cone generator at the given point (see Fig. 5). The difference of the mentioned angles causes rotation of the jet helix around its axis. Such a rotating helical jet is suggested by Rani et al. (2014) to interpret the observed alternation of intervals of strong positive and negative correlation between PA_{in} values and γ-ray flux density. We have shown that both ballistic and non-ballistic jets (Section 4) satisfy the observed picture of correlation. It is important to note that γ-rays are produced at smaller distance from the black hole than distance corresponding to the observed position of the VLBI-core (see, e.g., Fuhrmann et al. 2014) and especially distance of the feature for which PA_{in} is measured. Therefore it is quite possible that there is a difference between azimuth angles φ (φ indicates the feature orientation relative to a plane containing the line of sight and cone's axis) of these two jet regions for the same observation time. This difference strongly affects both the correlation coefficient κ of the mentioned values and duration of the interval when this κ is observed.

The contradictory results of kinematic studies of the S5 0716+71 jet (Bach et al. 2005; Britzen et al. 2009; Rastorgueva et al. 2011; Rani et al. 2015) are also easily explained by the helical jet model. According to Gomez et al. (1994), the stationary features observed by Britzen et al. (2009) are to be explained by the bent jet trajectory, and fast-moving features (Bach et al. 2005) can be caused by shock waves passing along the jet. In Section 5 we show that available differences in the apparent speed β_{app} of features at different observational epochs (Rastorgueva et al. 2011; Rani et al. 2015) are caused by difference in their azimuth angles. The ratio of β_{app} allows us to define the angle p at which the feature moves relative to the cone generator and to estimate the physical speed of jet features β. It has been obtained that in the case of the non-ballistic jet the angle between the feature velocity vector and the line of sight θ can reach small values (parts of a degree) what at a certain value β leads to the observed high apparent speeds of components (Rani et al. 2015). Such a small θ value cannot be obtained for the ballistic jet with geometric parameters estimated in Section 2, just as and the maximum value estimated at 11° (Rastorgueva et al. 2011).

7 CONCLUSIONS

We suggest the helical structure of the blazar S5 0716+71 parsec-scale jet. It allows us:

- to explain periodic variations of the inner jet position angle PA_{in}, the long-term flux variability in the radio and optical ranges;
- to coordinate different periods of long-term variability of the mentioned values between themselves;
- to explain alternation of time intervals of positive and negative correlation between the γ-ray flux and PA_{in};
- to bring into agreement available contradictory results of kinematic studies of the S5 0716+71 jet features;
- to explain the high apparent speed of jet components.

Within the considered jet model the following parameters were found:

- helical jet matter is located on the surface of the imaginary cone with the half-opening angle $\xi = 1°$ and angle between the cone axis and the line of sight $\theta_0 = 5.3°$. This result does not depend on the motion nature of jet components;
- distance from the VLBA-core to the cone's apex is about 2.5 pc;
- non-ballistic motion of jet features with the pitch angle $p = 5.5°$. This gives greater interval of possible values of the θ than for ballistic motion where $\theta = \theta_0 \pm \xi$;
- low constraint on the physical speed of jet features $\beta \geq 0.999$;
- it was concluded that the pitch angle differs from the angle ψ between the tangent to the helix and the cone generator at the given point.

Advantages of the helical jet model:

- it does not depend on mechanisms forming the helix;
- it self-consistently explains different observed properties of the blazar S5 0716+71 and its jet;
- the model may be applied to other blazars having both similar and different properties as compared to S5 0716+71. For example, a constant value of PA_{in} can be caused by either $\psi = p$ or insufficient flux density for recording jet features which velocity vector makes up larger angle with the line of sight.

Thus, the helical jet gives the interpretation of different observed properties of S5 0716+71. Herein, estimations of the half-opening angle of the jet's cone and distance of the VLBA-core from the black hole are in agreement with other independent estimations carried out by Pushkarev et al. (2009). Hence, variations of the Doppler factor strongly affect the long-term variability of the blazar S5 0716+71. It is generally accepted that in this case the period of light curve variability, with relativistic effects taking into account, reflects periodic processes occurring near the supermassive black hole (or binary black hole system). But in this paper we show that the motion of jet components influences duration of the variability period. In the case of the ballistic jet there is an increase of the period as the observational frequency decreases when the jet slows down. When features move at some pitch angle p then the period can be either absent at all (when $p = \psi$) or increases even without a decrease in the physical speed of jet features (when $p \neq \psi$). This is important to take into account when estimating physical parameters of the core, e.g. black hole mass. The helical jet also complicates a correlation picture of two different observed values and makes it strongly dependent on the jet geometry what hinders the detection of physical connection between these values. The study of correlation between radio and γ-ray variability (see, e.g., Fuhrmann et al. 2014) allows detecting locations of emitting regions. In addition, the jet geometry must also be taken into account. Note that from Figures 7 and 8, the correlation cannot be entirely absent. If it is observed then physical processes make a key contribution to variations of the studied values.

REFERENCES

Abraham Z., 2000, A&A, 355, 915
Abraham Z., Carrara E. A., 1998, ApJ, 496, 172
Bach U., Krichbaum T. P., Ros E., Britzen S., Tian W. W., Kraus A., Witzel A., Zensus J. A., 2005, A&A, 433, 815
Birkinshaw M., 1991, MNRAS, 252, 505
Blandford R. D., Königl A., 1979, ApJ, 232, 34
Britzen S. et al., 2009, A&A, 508, 1205
Bychkova V. S. et al., 2015, ARep, 59, 851
Bychkova V. S., Kardashev N. S., Boldycheva A. V., Gnedin Yu. N., Maslennikov K.L., 2006, ARep, 50, 802
Camenzind M., Krockenberger M., 1992, A&A, 255, 59
Caproni A., Abraham Z., 2004, MNRAS, 349, 1218
Caproni A., Abraham Z., Monteiro H., 2013, MNRAS, 428, 280
Conway J. E., Murphy D. W., 1993, ApJ, 411, 89
Dai Y., Wu J., Zhu Z.-H., Zhou X., Ma J., Yuan Q., Wang L., 2013, AJSS, 204, 22
Danforth C.W., Nalewajko K., France K., Keeney B. A., 2013, ApJ, 764, 57
Ferrari A., Trussoni E., Zaninetti L., 1981, MNRAS, 196, 1051
Fuhrmann L. et al., 2014, MNRAS, 441, 1899
Gabuzda D. C., Pushkarev A. B., Cawthorne T. V., 2000, MNRAS, 329, 1109
Gomez J. L., Alberdi A., Marcaide J. M., 1994, A&A, 284, 51
Gupta A. C., Fan J. H., Bai J. M., Wagner S. J., 2008, AJ, 135, 1384
Hardee P. E., 2000, ApJ, 533, 176
Hardee P. E., Norman M. L., 1988, ApJ, 334, 70
Komatsu E. et al., 2009, ApJS, 180, 330
Larionov et al., 2013, ApJ, 768, 40
Liao N. H., Bai J. M., Liu H. T., Weng S. S., Chen L., Li F., 2014, ApJ, 783, 83
Lister M. L. et al., 2013, AJ, 146, 120L
Liu X., Mi L., Liu B., Li Q., 2012, Ap&SS, 342, 465
Marscher A. P., Gear W. K., 1985, ApJ, 298, 114
McKinney J. C., Blandford R. D., 2009, MNRAS, 394, L126
Meier D. L., Koide S., Uchida Y., 2001, Sci, 291, 84
Montagni F., Maselli A., Massaro E., Nesci R., Sclavi S., Maesano M., 2006, A&A, 451, 435
Nesci R., Massaro E., Rossi C., Sclavi S., Maesano M., Montagni F., 2005, AJ, 130, 1466
Nilsson K., Pursimo T., Sillanpää A., Takalo L. O., Lindfors E., 2008, A&A, 487, L29
Pietilä H., 1998, AJ, 508, 669
Poon H., Fan J. H., Fu J. N., 2009, ApJSS, 185, 511
Pushkarev A. B., Kovalev Y. Y., Lister M. L., Savolainen T., 2009, A&A, 507, 33L
Pushkarev A. B., Hovatta T., Kovalev Y. Y., Lister M. L., Lobanov A. P., Savolainen T., Zensus J. A., 2012, A&A, 545, 113
Raiteri C. M. et al., 2003, A&A, 402, 151
Rani B., Krichbaum T. P., Marscher A. P., Jorstad S.G., Hodgson J. A., Fuhrmann L., Zensus J. A., 2014, AJ, 146, 120
Rani B., Krichbaum T. P., Marscher A. P., Hodgson J. A., Fuhrmann L., Angelakis E., Britzen S., Zensus J. A., 2015, A&A, 578, 123
Rastorgueva E. A., Wiik K. J., Bajkova A. T., Valtaoja E., Takalo L. O., Vetukhnovskaya Y. N., Mahmud M., 2011, A&A, 529, A2
Rastorgueva E. A., Wiik K. J., Savolainen T., Takalo L. O., Valtaoja E., Vetukhnovskaya Y. N., Sokolovsky K. V., 2009, A&A, 494, 5L
Savolainen T., Homan D. C., Hovatta T., Kadler M., Kovalev Y. Y., Lister M. L., Ros E., Zensus J. A., 2010, A&A, 512, 24
Sbarufatti B., Treves A., Falomo R., 2005, ApJ, 635, 173
Stalin C. S., Gopal-Krishna, Sagar R., Wiita P. J., Mohan V., Pandey A. K., 2006, MNRAS, 366, 1337
Stirling A. M. et al., 2003, MNRAS, 341, 405
Villata M., Raiteri C. M., 1999, A&A, 347, 30
Vol'Vach A. E. et al., 2009, ARep, 53, 777
Wagner S. J. et al., 1996, AJ, 111, 2187
Wu J., Zhou X., Ma J., Wu Z., Jiang Z., Chen J., 2007, AJ, 133, 1599